Results in Physics 9 (2018) 1233–1238

Contents lists available at ScienceDirect

Results in Physics

journal homepage: www.elsevier.com/locate/rinp

Fabrication and thermoelectric properties of Ca-Co-O ceramics with negative Seebeck coefficient

Chunlin Gong[a], Zongmo Shi[b], Yi Zhang[b], Yongsheng Chen[c], Jiaxin Hu[a], Jianjun Gou[a], Mengjie Qin[b], Feng Gao[b,*]

[a] Shaanxi Aerospace Flight Vehicle Design Key Laboratory, School of Astronautics, Nothwestern Polytechnical University, Xi'an 710072, PR China
[b] State Key Laboratory of Solidification Processing, MIIT Key Laboratory of Radiation Detection Materials and Devices, School of Material Science and Engineering, Northwestern Polytechnical University, Xi'an 710072, PR China
[c] Department of Mechanical and Automation Engineering, The Chinese University of Hong Kong, Shatin, N.T., Hong Kong Special Administrative Region

ARTICLE INFO

Keywords:
Thermoelectric ceramic
Negative Seebeck coefficient
Annealing
Reducing atmosphere

ABSTRACT

Ca-Co-O ceramics is typically p-type thermoelectric materials and possesses positive Seebeck coefficient. In this work, n-type Ca-Co-O ceramics with negative Seebeck coefficients were fabricated by sintering and annealing in a reducing atmosphere. The microstructures and thermoelectric properties of the ceramics were investigated. The results show that the carrier concentration and the carrier mobility dramatically increase after the samples were annealed in the reducing atmosphere. The electrical resistivity increases from 0.0663 mΩ·cm to 0.2974 mΩ·cm, while the negative Seebeck coefficients varies from −24.9 μV/K to −56.3 μV/K as the temperature increases from 323 K to 823 K, and the maximum power factor (*PF*, 1.536 mW/m·K^2) is obtained at 623 K. The samples have n-type thermoelectric properties with large *PF* values and *ZT* value (*ZT* = 0.39, 823 K). The unusual results will pave a new way for studying Ca-Co-O thermoelectric ceramics.

Introduction

Metal oxide based thermoelectric generation is expected to make considerable power conversion efficiency improvements in the satellite and spaceship [1–3]. During supersonic and hypersonic flight, metal oxide based thermoelectric material has potential to transfer aero-heating energy into essential electrical energy for avionics. Using metal oxides has several advantages, such as environmental friendliness, high chemical stability at high temperatures in air, and long service life [4–6]. Ca-Co-O system is typically p-type thermoelectric material, which includes many different compounds, such as $CaCo_2O_4$, $Ca_2Co_2O_5$, $Ca_3Co_4O_9$ ($Ca_9Co_{12}O_{28}$), and $Ca_3Co_2O_6$ [7,8]. Recently, owing to their excellent thermoelectric performance, $Ca_3Co_4O_9$ and $Ca_3Co_2O_6$ have attracted great attention than the other compounds [9]. The misfit-layered $Ca_3Co_4O_9$ consists of two alternating subsystems, a rock salt type Ca_2CoO_3 layer and a CdI_2 type CoO_2 sheet. Ca_2CoO_3 layers play an important role in generating thermopower and CoO_2 sheets determine the thermal conductivity [7]. Meanwhile, the perovskite $Ca_3Co_2O_6$ consists of parallel one-dimensional (1D) $Co_2O_6^{6-}$ chains separated by Ca^{2+} ions, possessing rich magnetic, electric and thermoelectric properties [10]. Besides, the phase equilibrium study has confirmed the absence of the intermediate complex oxides inside the Ca-Co-O system at 1373 K in air. Nowadays, most of the investigated Ca-Co-O materials have high positive Seebeck coefficient as p-type semiconductors [11–13], and a lot of effective methods have been taken to enhance the properties of Ca-Co-O thermoelectric materials, such as doping, introducing nano-phases, and using novel sintering process [4–8].

For high temperature applications in air, thermoelectric (TE) modules are fabricated and characterized with various combinations of p-type and n-type TE oxide materials as segmented TE legs, such as p-type Ca-Co-O and n-type $CaMnO_3$, $SrTiO_3$, etc. [12–15]. However, the difference in thermal expansion coefficient between p-type Ca-Co-O and n-type materials at high temperatures results in thermal stress in the connector lug and connection problems between the legs and electrodes. Thus, it is imperative to develop compatible p-legs and n-legs with similar composition to mitigate these problems and simplify the preparation process [13]. Due to the contradicting physical characteristics of the p-type and n-type TE oxide materials, it is difficult to prepare a compound with both p-type and n-type thermoelectric performance.

In our previous work, we fabricated La-Bi co-doped $SrTiO_3$ ceramics with negative Seebeck coefficient by annealing with graphite in argon atmosphere, the electrical resistivity of the ceramics reduce 6–7 orders of magnitude, and the absolute Seebeck coefficient decreases

* Corresponding author.
E-mail address: gaofeng@nwpu.edu.cn (F. Gao).

https://doi.org/10.1016/j.rinp.2018.04.044
Received 12 March 2018; Received in revised form 16 April 2018; Accepted 16 April 2018
Available online 21 April 2018

dramatically with adding the high content (x > 20) of Ag nanoparticles [14,15], which demonstrate n-type thermoelectric materials can be obtained by sintering and annealing in reducing atmosphere even for oxide materials with high electrical resistivity. In this work, we prepare (Ag, La) co-doped Ca-Co-O ceramics by the conventional solid state reaction method and process them in a similar fashion. n-type semi-conductive Ca-Co-O thermoelectric ceramics are obtained and the mechanism has been discussed.

Experimental method

Ceramic samples of a general formula $Ca_{2.55}Ag_{0.3}La_{0.15}Co_4O_9/x$ *wt*% Ag (x = 0, 10) were synthesized by conventional solid state reaction, using $CaCO_3$ (99.5%), Co_2O_3 (99.7%), $AgNO_3$, La_2O_3, and Ag nanoparticles (average size ~50 nm) as raw materials. Ag nanoparticles were used to form a percolating network and to increase the electrical conductivity [14]. The precursor raw materials were weighted in stoichiometric ratios and ball milled with ethanol for 24 h, followed by drying at 313 K and calcining in air at 1203 K for 4 h. The calcinated powder was pressed into pellets (Φ30 mm × 4 mm) and sintered at 1473 K in flowing argon gas for 10 h. Then an annealing process was performed at 1373 K with graphite in argon atmosphere (Ar + C) for 8 h. The heating rate was 5 °C/min, the cooling rate, 5 °C/min, and the argon flow rate, 20 ml/min. Bars of 15 mm × 4 mm × 3 mm were cut and polished to test thermoelectric properties.

Densities of the samples were measured using the Archimedes method. Phases of the as-synthesized particles and ceramics were examined by XRD (Panalytical X'Pert PRO, Holland) using Cu Kα radiation with a step size of 0.02°. Microstructures were observed by SEM (Quanta 600 FEG, United States), and samples components were examined by EDS (INCA, United Kingdom). The surface composition of the samples using the powder of the sintered ceramics was characterized by X-ray photoelectron spectroscopy (XPS, Kratos Axis Ultra DLD) using Al Kα radiation. The electrical resistivity and Seebeck coefficients were measured in the temperature range between 373 and 823 K using LINSEIS LSR3/1100 equipment. The thermal conductivity was obtained from measurements of the thermal diffusivity (λ) and specific capacity (C_p) with a laser flash apparatus (Netzsch LFA 427, Netzsch, Selb, Germany). ZT value is calculated by $(S^2T)/(\rho\kappa)$. The carrier concentration and mobility were tested at room temperature using VTHM-1 Hall Effect equipment.

Results and discussion

Microstructure of Ca-Co-O/xAg ceramics

Fig. 1 shows the XRD patterns of the calcinated powders and sintered ceramics before and after annealing. The diffraction patterns, when compared with JCPDS data, show that there are $Ca_3Co_4O_9$, $Ca_3Co_2O_6$, CaO, and metallic Ag phases in the calcinated powders, while $Ca_3Co_4O_9$, $Ca_3Co_2O_6$, CoO, CaO, and metallic Ag phases are present in the ceramics before annealing. After the samples were annealed with graphite in argon atmosphere, there exist $Ca_3Co_2O_6$, CoO, CaO, and metallic Ag phases with an increase of CoO phase. The phase diagram of Ca-Co-O system shows in thermodynamics equilibrium that there are different phases at different temperatures [7]. When the temperature is above 1166 K, $Ca_3Co_4O_9$ and CoO co-exist in the system, which transforms to $Ca_3Co_2O_6$ and CoO when the temperature reaches 1199 K. At temperatures above 1299 K, $Ca_3Co_2O_6$ is decomposed to CaO and CoO. The amounts of CoO are 17.1% and 26.9% before and after annealing. Although the samples consist of multiphase CaO, CoO, Ag and $Ca_3Co_2O_6$, the complex Ca-Co-O-based ceramics with negative Seebeck coefficients can be prepared. The relevant equations are as follows

$$Ca_3Co_4O_9 \xrightarrow{1199\ K} Ca_3Co_2O_6 + 2CoO + O_2(g) \quad (1)$$

$$2Ca_3Co_2O_6 \xrightarrow{1299\ K} 6CaO + 4CoO + O_2(g) \quad (2)$$

Fig. 2 shows the field emission scanning electron microscopy (FESEM) images from fractured surfaces of CALC/Ag ceramics before and after annealing. There are few voids visible on the samples, the average particle size of Ca-Co-O before annealing (~5 μm) is larger than that of the annealed (~2 μm). Additionally, the sintering temperature was higher than the melting point of Ag nanoparticles, thus it was expected the Ag particles had melt in the process and aggregated to form networks, which would promote the mass transfer and lead to densification during the sintering process. The bulk density of the sintered CALC/Ag sample is 5.19 g/cm^3, and after annealing it increases to 5.47 g/cm^3.

Ca-Co-O/xAg samples were analyzed using X-ray photoelectron spectroscopy (XPS). The full XPS spectra of the samples are shown in Fig. 3. XPS results from Ca-Co-O compounds show the statistic average content of the oxygen vacancies resulted from the whole Ca-Co-O ceramics powders, not just some certain substance, such as CaO, CoO or $Ca_3Co_2O_6$.

In the Fig. 3(a), the Ca 2*p*, Ca 2*s*, Co 2*p*, O 1*s* peaks are observed. Furthermore, Ag 3*d* and Ag 3*p* peaks obviously exist in Fig. 3(b), the result shows that the Ag element exists in the elemental state. As XPS patterns show, there is no Co 2*p* peak before annealing, but after annealing the binding energy positions of Co $2p_{3/2}$ and Co $3p_{1/2}$ spectra yield two peaks, at 777.9 eV and 792.9 eV. A narrow scan of Co 2*p* indicates that Co has an oxidation state corresponding to Co^{2+}. Co 2*p* peaks of all samples show a multiplet feature indicating the existence of different valence states of Co [15]. These results indicate that there are two modes that can be used to compensate electric charges in Ca-Co-O

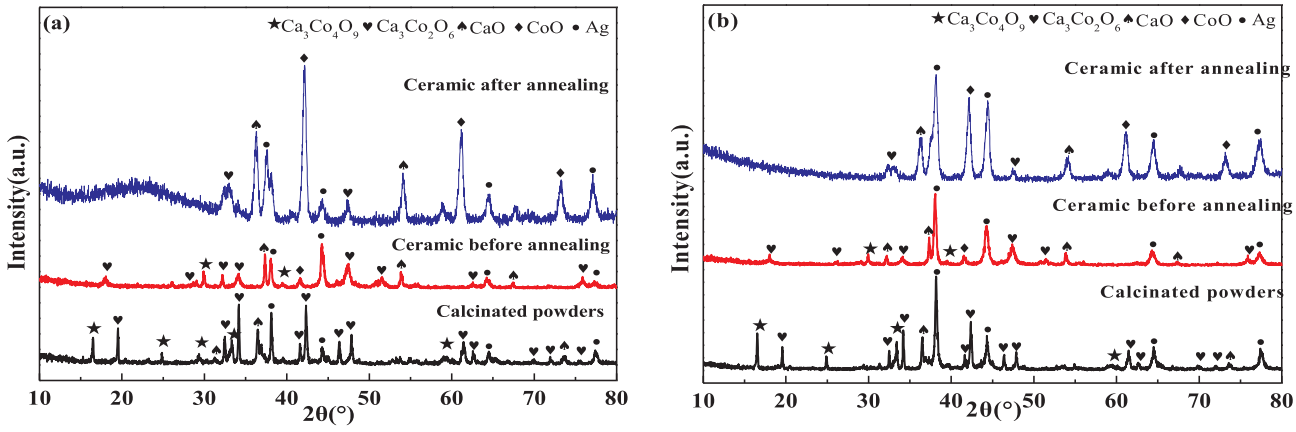

Fig. 1. XRD patterns of ceramics (a) CALC; (b) CALC/Ag.

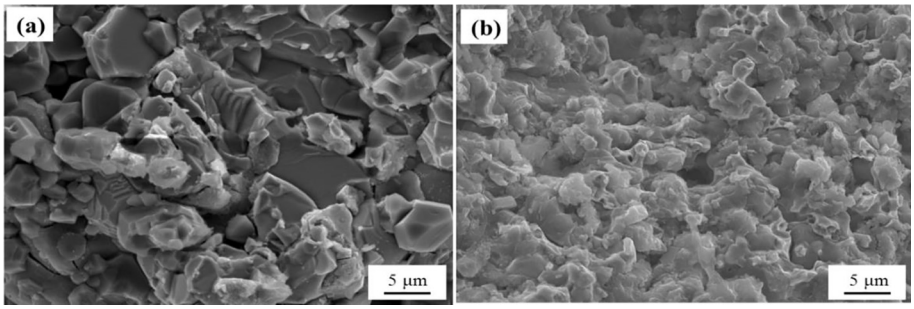

Fig. 2. SEM micrographs of CALC/Ag ceramics (a) before and (b) after annealing.

system. One is Co ions with different chemical valence, and the other, the oxygen vacancies ($V_{\ddot{O}}$). In this work, it reveals that ($V_{\ddot{O}}$) compensates for redundant charges.

Fig. 4 shows O 1*s* spectra before and after annealing in Ar + C atmosphere, which yields two peaks. The position of the O 1*s* shows a tendency of decreasing binding energy, from samples before and after annealing. The binding energy peak is shifted to a lower energy position for the samples annealed in Ar + C. The stronger peak is located in 528.74 eV, which is related to oxygen in the crystal structure. The peak located in 530.54 eV (due to the chemical adsorption), which may be assigned to less electron-rich oxygen species [16–18].

Under different oxygen partial pressures, oxygen species may

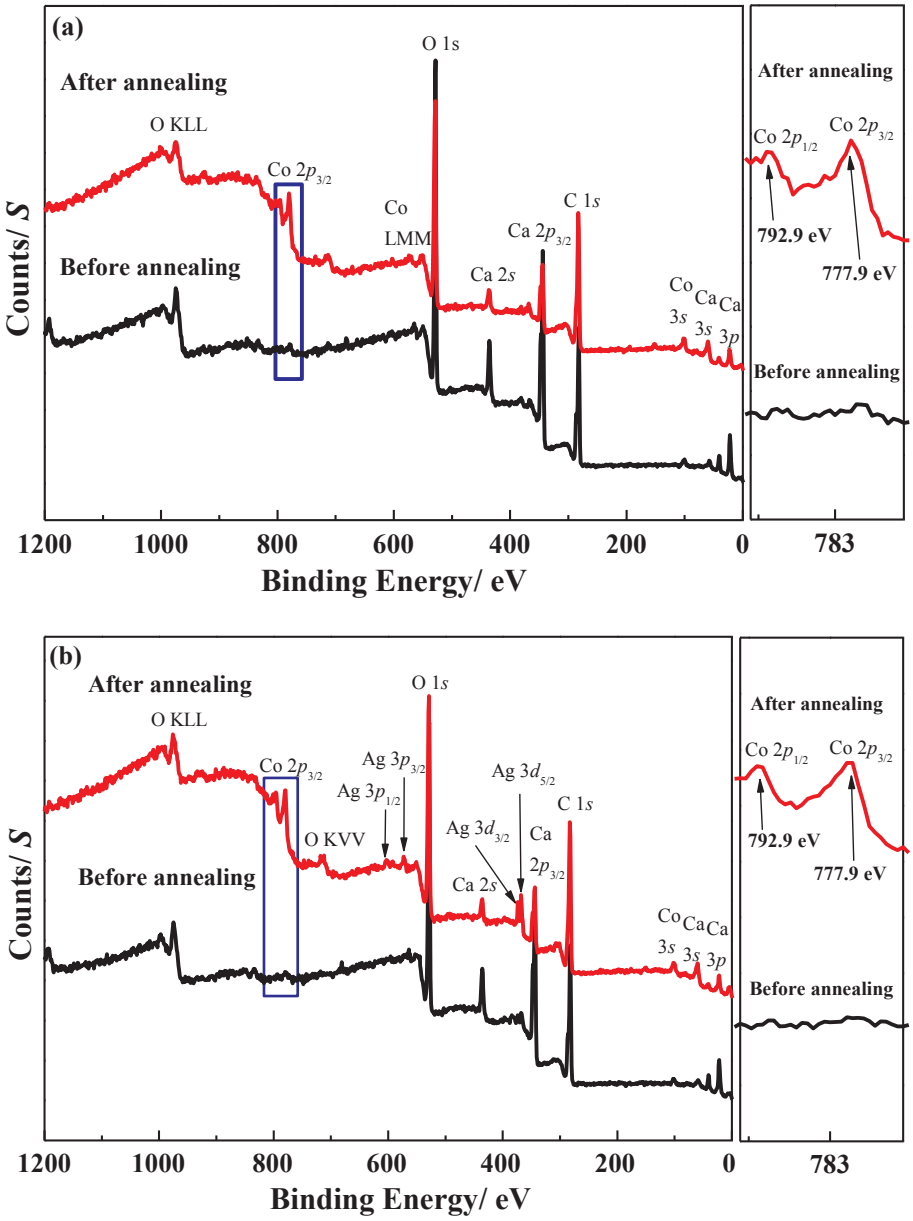

Fig. 3. XPS of ceramics before and after annealing (a) CALC; (b) CALC/Ag.

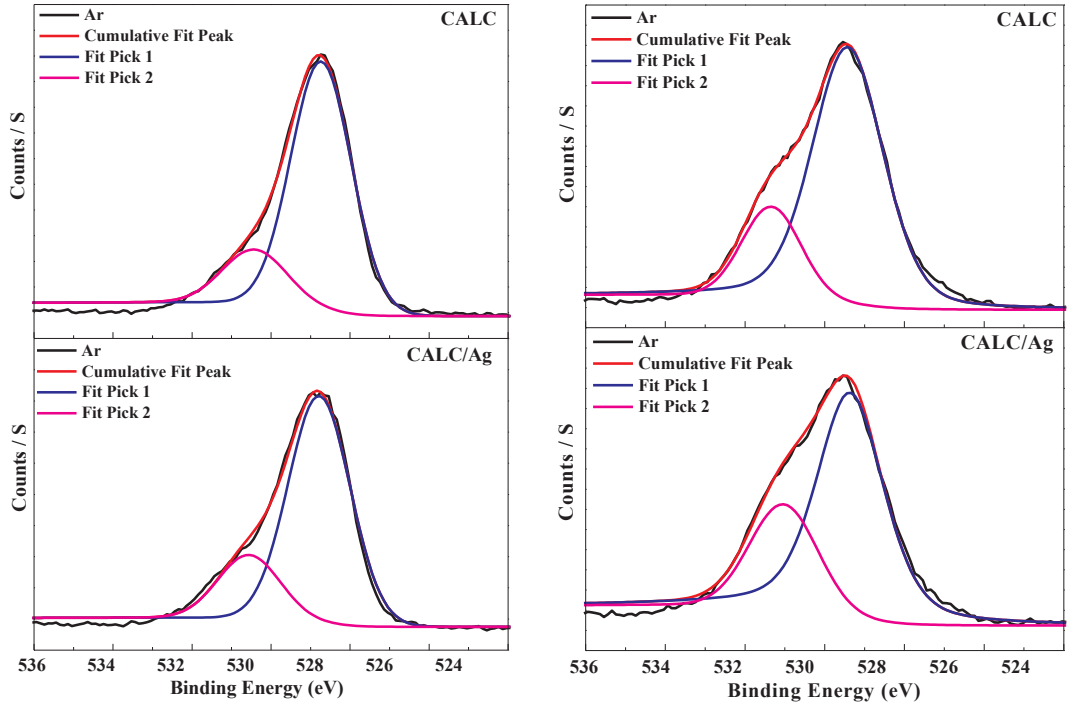

Fig. 4. XPS spectra of the O 1*s* of samples.

evolve. A general scheme is shown below [19–22]:

$$O_2(gas) \xrightarrow{+e^-} O_2^- \xrightarrow{+e^-} O_2^{2-} \leftrightarrow 2O^1 \xrightarrow{+2e^-} 2O^{2-}(\text{lattice}) \quad (3)$$

As can be seen from equation (3), the stronger peak associated with O^{2-} ions, which were related to oxygen in the CoO_2 layers composed of edge-sharing CoO_6 octahedra, the absorbing peak is due to an intermediate oxidation state which is related to $V_{\ddot{O}}$. The relative content of $V_{\ddot{O}}$ can be calculated by the ratio between the intensity of fitting peak 2 and the summed intensities of fitting peaks 1 and 2 (abbreviated as *y*). The calculated results are shown in Table 1. It can be seen that not only the value increased after annealing in Ar + C, but also the ratio increased with Ag addition content, indicating that more oxygen vacancies formed and stabilized during the annealing process.

Thermoelectric properties of Ca-Co-O/Ag ceramics

Fig. 5 shows the electrical resistivity (ρ) and Seebeck coefficient (*S*) of CALC and CALC/Ag, as a function of temperature in the range between 323 K and 823 K. With increasing temperature, the electrical resistivity of CALC/Ag increases from 0.0663 mΩ·cm to 2.974 mΩ·cm, which presents a metallic characteristic. Compared to the values in other reports on Ca-Co-O system, this ρ value is much lower. It shows that the Ca-Co-O system, which was annealed in a reducing atmosphere, transforms from a semi-conductor to a metal. At the same time, with the increasing temperature, the enhanced thermal vibrations of crystal the lattice elevate the electron scattering effect and reduce the carrier mobility, thus resulting in the increasing resistivity [18–21].

The Seebeck coefficients are negative and their absolute values increase monotonically with temperature for the samples CALC and CALC/Ag. Specifically, the CALC/Ag has an *S* value of −56.3 μV/K at 823 K. It is well known that Ca-Co-O materials are p-type semi-conductors when sintered in oxidizing atmospheres. However, annealed in the reducing atmosphere, Ca-Co-O samples have become n-type semiconductors. Ca-Co-O compounds show tunable p-type and n-type conductivity under O rich and O poor conditions, which means that semiconductive characteristics transform from p-type to n-type by the influence of the annealing atmosphere. The first reason is that La^{3+} doping can produce a large amount of Ca vacancies (V''_{Ca}), leading to higher mobility of the lattice oxygen at high temperatures. The second reason is that the different valence states of Co ions can affect the mobility of electrons in the CoO_2 layers. The third reason is that large amount of oxygen vacancies are generated in reducing atmosphere, and the free electrons released by $V_{\ddot{O}}$ ionization in low oxygen partial pressure [20–22]. The defect reaction equations are shown as follows:

$$Ca_3Co_4O_9 \xrightarrow{La_2O_3} 2La_{Ca}^{\cdot} + V''_{Ca} + 9O_O^x + 4Co_{Co}^x \quad (4)$$

$$2Co_{Co}^x + O_O^x \xrightarrow{\text{reduction}} 2Co'_{Co} + V_{\ddot{O}} + \frac{1}{2}O_2 \quad (5)$$

$$O_O^x = V_{\ddot{O}} + 2e' + \frac{1}{2}O_2 \quad (6)$$

Fig. 6 shows the power factors (*PF*) calculated by S^2/ρ, as a function of temperature in the range between 323 K and 823 K. Based on the above results, with increasing temperature, the *PF* value increases initially and reaches a maximum value of 1.536 mW/m·K^2 at 623 K, then decreases. It is worth noting that the *PF* values from this work are 1.6–4.5 times larger than that of p-type $Ca_3Bi_{0.1}Ba_{0.07}Co_4O_9$ [22], $Ca_3Co_4O_9$/Ag [5], and $Ca_{2.8}Lu_{0.2}Co_4O_9$ [9] thermoelectric ceramics, and 2.2–4.5 times larger than that of n-type $Sr_{0.9}La_{0.1}TiO_3$ [14], $[Ca_{0.95}(Dy_{1/2}Na_{1/2})_{0.05}]MnO_3$ [23], and $Zn_{97}Al_2GaO_{100}$ [24] materials, as shown in Table 2. At the same time, this variation trend of *PF* can easily observed in other thermoelectric materials, such as $Bi_2(Te_{0.94}Se_{0.06})_3$ annealed in hydrogen [25] and Ca_{3-x} $Pb_xCo_2O_6$

Table 1
The ratio of fit peak 2 and (fit peak 1 + fit peak 2).

Samples	Before annealing	After annealing	Δ*y*	Δ*y*%
CALC	18.7%	20.5%	1.8%	9.62
CALC/Ag	21.8%	27.9%	6.1%	27.98

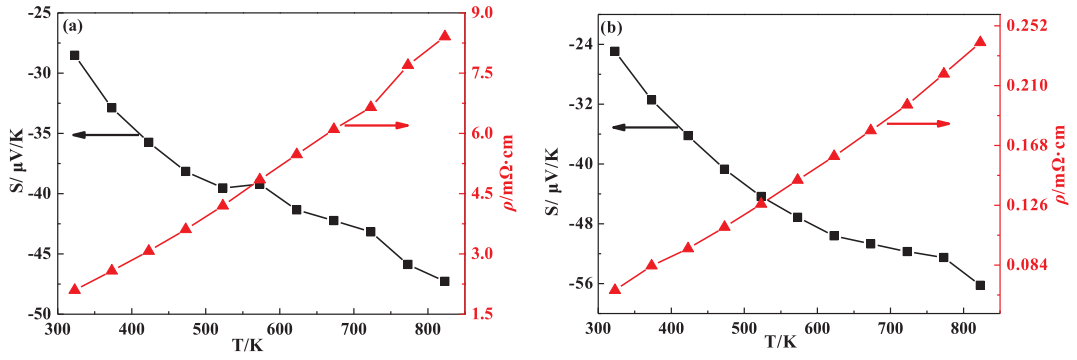

Fig. 5. Electrical resistivity and Seebeck coefficient of the samples (a) CALC and (b) CALC/Ag.

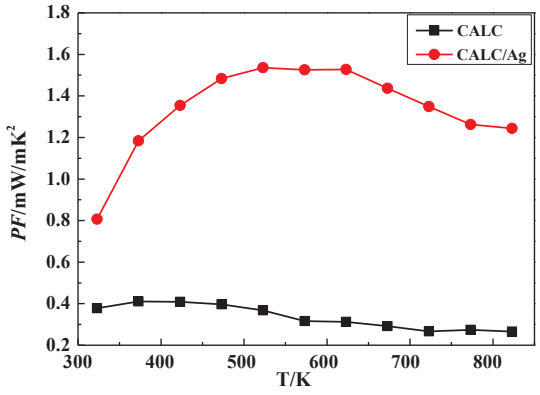

Fig. 6. Power factors (*PF*) of the samples.

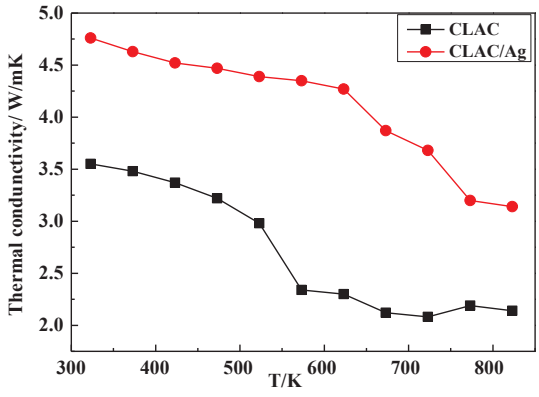

Fig. 7. Thermal conductivity of the samples.

Table 2
The thermoelectric properties at 623 K of different p-type and n-type materials.

Composition	TE Type	ρ(mΩ·cm)	*S*(μV/K)	*PF* (mW/m·K²)	*ZT*	References
$Ca_{2.9}Ba_{0.1}Co_4O_9$	p	8.3	170	0.93	0.20	[22]
$Ca_3Co_4O_9$/Ag	p	11	165	0.34	0.19	[5]
$Ca_{2.8}Lu_{0.2}Co_4O_9$	p	12	185	0.32	0.36	[9]
$Sr_{0.9}La_{0.1}TiO_3$	n	12	−225	0.67	0.14	[14]
$[Ca_{0.95}(Dy_{1/2}Na_{1/2})_{0.05}]MnO_3$	n	8.7	−252	0.35	0.24	[23]
$Zn_{97}Al_2GaO_{100}$	n	3.5	−220	0.23	0.37	[24]
CALC/Ag	n	0.16	−50	1.54	0.39	This work

(x = 0–0.3) [26].

It is reported that a potential barrier will be created from band bending upon metallic addition in the semiconductor matrix [27]. Such a barrier acts as an energy filter from which low-energy electrons are strongly scattered, while high-energy electrons remain almost unaffected. This kind of filtering effect leads to an increase of the average carrier energy. As a result, the Seebeck coefficient is enhanced. In this work, Ag addition probably induces the filtering of low energy carriers, resulting in the enhancement of the Seebeck coefficient.

The thermal conductivity (κ) of samples is shown in Fig. 7. It reveals that the thermal conductivities of both CALC and CALC/Ag ceramics decrease with increasing temperatures. The thermal conductivities of CALC and CALC/Ag samples are in the range of 2.1–3.5 W/mK^{-1} and 3.5–4.75 W/mK^{-1}, respectively. Compared with CCO single crystals, CALC/*x*Ag possess higher thermal conductivity [8], the κ increased slightly for complex ceramics annealed in Ar + C atmosphere. Meanwhile, the thermal conductivity of CALC/Ag samples is higher than that of the CALC samples. Therefore, weakening phonons scattering with 10 wt% secondary-phase nanoparticles added is responsible for the observed higher thermal conductivity. The thermoelectric figure of merit (*ZT*) for Ca-Co-O ceramics is shown in Fig. 8. With the temperature increasing, *ZT* values of the samples increase and reach 0.39 at 823 K for CACL/Ag, because of the lower electrical resistivity and higher Seebeck coefficient.

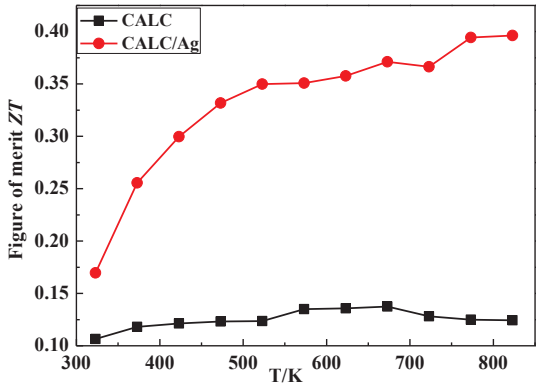

Fig. 8. Figure of Merit *ZT* of the samples.

Hall coefficients were measured in 8000 Gs magnetic field, the results are shown in Table 3. On one hand, all samples possess the n-type semi-conductive properties and the electrical resistivity decreases by 7–8 orders of magnitude. On the other hand, the carrier concentration and the carrier mobility increase dramatically after the samples were annealed in reducing atmosphere. Added Ag nanoparticles can augment carrier concentration and turn down the carrier mobility of CALC, which results in the lower electrical resistivity, enhanced power factor value and *ZT*. Comparing with the other n-type oxide thermoelectric ceramics, *ZT* value of the CACL/Ag sample also shows a high level (Table 2), which demonstrates that CALC/Ag compound is a good candidate material for n-type thermoelectric applications.

Table 3
Hall effect results of samples before and after annealing.

Conductions	Samples	Electrical resistivity (mΩ·cm)	Carrier concentration (1/cm^3)	Mobility (cm^2/V/S)
Before annealing	CALC	1.306×10^8	1.3710×10^{12}	0.4401
	CALC/Ag	2.7813×10^5	1.9579×10^{17}	0.2126
After annealing	CALC	0.1032	4.7763×10^{21}	8.7972
	CALC/Ag	0.0441	7.6986×10^{21}	3.1602

Conclusions

Ca-Co-O thermoelectric ceramics with negative Seebeck coefficient were prepared by sintering and annealing in reducing atmosphere. The samples possess the n-type semi-conductive characteristics. The carrier concentration and the carrier mobility increase dramatically after samples were annealed in reducing atmosphere. Ag nanoparticles can increase carrier concentration and decrease the carrier mobility. With increasing temperature, the electrical resistivity of CALC/Ag increases from 0.0663 mΩ·cm to 0.2974 mΩ·cm, the Seebeck coefficient varies from −24.9 μV/K to −56.3 μV/K, which should be ascribed to the change in carrier concentration and oxygen vacancy. The large *PF* value of 1.536 mW/m·K^2 at 623 K and the maximum *ZT* value of 0.39 is obtained at 823 K, which makes CALC/Ag compound a good candidate material used for n-type thermoelectric applications.

Acknowledgments

This work was supported by the National Natural Science Foundation of China (No. 51672219), Foundation of National High Technology Research and Development Program (No. 2015AA0172), Fundamental Research Fund for the Central Universities (No. G2016KY0302), the “111” Project (No. B08040), and the Research Foundation of the State Key Laboratory of Solidification Processing (NWPU), China (No. 137-QP-2015).

References

[1] Terasaki I. Transport properties and electronic states of the thermoelectric oxide $NaCo_2O_4$. Phys B 2003;328:63–7.
[2] Yin LH, Ang R, Li LJ, Zhao BC, Fu YK, Zhu XB, Yang ZR, Song WH, Sun YP. Thermoelectric properties of sol–gel derived cobaltite $Bi_2Ca_{2.4}Co_2O_y$. Phys B 2011;406:2914–8.
[3] Wang Y, Sui Y, Cheng JG, Wang XJ, Su WH, Liu XY, Fan HJ. Doping-induced metal-insulator transition and the thermal transport properties in $Ca_{3-x}Y_xCo_4O_9$. J Phys Chem C 2010;114:5174–81.
[4] Li CH, Guo DL, Li KJ, Shao B, Chen DM, Ma YL, Sun JC. Excellent thermoelectricity performance of p-type SnSe along b axis. Phys B 2018;530:264–9.
[5] Boyle C, Liang L, Chen Y, Prucz J, Cakmak E, Watkins TR, Lara-Curzio E, Song XY. Competing dopants grain boundary segregation and resultant seebeck coefficient and power factor enhancement of thermoelectric calcium cobaltite ceramics. Ceram Int 2017;43:11523–8.
[6] Ohta H, Sugiura K, Koumoto K. Recent progress in oxide thermoelectric materials: p-type $Ca_3Co_4O_9$ and n-type $SrTiO_3$. Inorg Chem 2008;47:8429–36.
[7] Fergus JW. Oxide materials for high temperature thermoelectric energy conversion. J Eur Ceram Soc 2012;32:525–40.
[8] Kahraman F, Madre MA, Rasekh S, Salvador C, Bosque P, Torre MA, Diez JC, Sotelo A. Enhancement of mechanical and thermoelectric properties of $Ca_3Co_4O_9$ by Ag addition. J Eur Ceram Soc 2015;43:3835–41.
[9] Nong NV, Liu CJ, Ohtaki M. High-temperature thermoelectric properties of late rare earth-doped $Ca_3Co_4O_{9+\delta}$. J Alloy Compd 2011;509:977–81.
[10] Nong NV, Ohtaki M. Power factors of late rare earth-doped $Ca_3Co_2O_6$ oxides. Solid State Commun 2006;139:232–4.
[11] Li HZ, Li RP, Liu JH, Huang MJ. Convergence of valence bands for high thermoelectric performance for p-type InN. Phys B 2015;479:1–5.
[12] Chen S, Cai KF, Zhao WY. The effect of Te doping on the electronic structure and thermoelectric properties of SnSe. Phys B 2012;407:4154–9.
[13] Yang HX, Nie CJ, Shi YG, Yu HC, Ding S, Liu YL, Wu D, Wang NL, Li JQ. Structural phase transitions and sodium ordering in $Na_{0.5}CoO_2$: a combined electron diffraction and Raman spectroscopy study. Solid State Commun 2005;134:403–8.
[14] Qin MJ, Gao F, Wang M, Zhang CC, Zhang QQ, Wang L. Fabrication and high-temperature thermoelectric properties of Ti-doped $Sr_{0.9}La_{0.1}TiO_3$ ceramics. Ceram Int 2016;42:16644–9.
[15] Qin MJ, Gao F, Wang M, Wang L, Dong GG, Huang XX. Microstructure and enhanced seebeck coefficient of textured $Sr_3Ti_2O_7$ ceramics prepared by RTGG method. Ceram Int 2016;42:13748–54.
[16] Kumar RS, Rekhi S, Prabhakaran D, Somayazulu M, Kim E, Cook JD, Stemmler T, Boothroyd AT, Chance MR, Cornelius AL. Structural studies on $Na_{0.75}CoO_2$ thermoelectric material at high pressures. Solid State Commun 2009;149:1712–6.
[17] Su LS, Gan YX, Zhang LH. Thermoelectricity of nano composites containing TiO_2-CoO coaxial nano cables. Scr Mater 2011;64:745–8.
[18] Dahshan A, Hegazy HH, Aly KA, Sharma Pankaj. Semiconducting Ge-Se-Sb-Ag chalcogenides as prospective materials for thermoelectric applications. Phys B 2017;526:117–21.
[19] Wu JM, Chen LJ, Yang XB, Zhao YJ. Tuning p/n conductivity in wurtzite transition metal monoxide: role of native defects in CoO and MnO. Phys Lett A 2014;378:2635–9.
[20] Gong CL, Dong GG, Hu JX, Chen YS, Qin MJ, Yang SJ, Gao F. Effect of reducing annealing on the microstructure and thermoelectric properties of La-Bi co-doped $SrTiO_3$ ceramics. J Mater Electron 2017;28:14893–900.
[21] Yang WC, Zhang HC, Tao JQ, Zhang DD, Zhang DW, Wang ZH, Tang GD. Optimization of the spin entropy by incorporating magnetic ion in a misfit-layered calcium cobaltite. Ceram Int 2016;42:9744–8.
[22] Zhang FP, Liang L, Lu QM, Li TX, Zhang X, Zhang JX, Xiao YS. Preparation and thermoelectric transport properties of Ba-, La- and Ag-doped $Ca_3Co_4O_9$oxide materials. J Rare Earths 2013;31:778–83.
[23] Zhou YC, Wang CL, Su WB, Liu J, Wang HC, Li JC, Li Y, Zhai JZ, Zhang YC, Mei LM. Electrical properties of Dy^{3+}/Na^+ Co-doped oxide thermoelectric $[Ca_{1-x}(Na_{1/2}Dy_{1/2})_{(x)}]MnO_3$ ceramics. J Alloy Compd 2016;680:129–32.
[24] Brockway L, Vasiraju V, Sunkara MK, Vaddiraju S. Engineering efficient thermoelectrics from large-scale assemblies of doped ZnO nanowires: nanoscale effects and resonant-level scattering. ACS Appl Mater Interface 2014;6:14923–30.
[25] Yamashita O, Tomiyoshi S. Bismuth telluride compounds with high thermoelectric figures of merit. J Appl Phys 2003;93:368–74.
[26] Song JY, Zhao BC, Huang YN, Qin YF, Song WH, Sun YP. Tuning of conductive type and magnetic properties of $Ca_3Co_2O_6$ ceramics through Pb-doping. J Am Ceram Soc 2017;100:3589–98.
[27] Faleev SV, Leonard F. Theory of enhancement of thermoelectric properties of materials with nanoinclusions. Phys Rev B 2008;77:214–304.